INSTABILITY OF A MECHANICAL SYSTEM INDUCED BY AN IMPINGING FLUID JET*

by

Walter T. Feldt,[1] S. Nemat-Nasser,[2] S. N. Prasad[3] and George Herrmann[4]

Department of Civil Engineering
The Technological Institute
Northwestern University
Evanston, Illinois

---

* This research was supported by the National Aeronautics and Space Administration under Grants NsG 605 and NGR 14-007-067.

[1] Graduate Student.

[2] Presently Assistant Professor, Department of the Aerospace and Mechanical Sciences, University of California at San Diego.

[3] Presently Assistant Professor, Department of Civil Engineering, University of Mississippi, University, Mississippi.

[4] Professor.

TABLE OF CONTENTS

ABSTRACT

This study is concerned with the theoretical and quantitative experimental determination of critical loads which separate stable from unstable states of equilibrium of a mechanical system subjected to the action of an impinging fluid jet. It was found that the type of loss of stability is determined by the properties of the surface upon which the jet impinges. For a smooth surface, stability was lost by divergence (static buckling), whereas for a surface with a screen of certain mesh size, stability was lost by flutter (oscillations with increasing amplitudes). The experimental results have been compared with a theoretical stability analysis of this nonconservative system and a satisfactory correlation of numerical values is shown to exist, particularly if the peculiar effects of damping are accounted for.

LIST OF SYMBOLS

a,b,c	=	coefficients in frequency equation
a_1,a_2,b_1,b_2 $c_1,c_2,d_2,\ell_1,\ell_2$	=	linear dimensions of the model
A_n	=	nth amplitude
A,B,C,D	=	constants
A^*	=	modified value of A
$A_1,A_2,\ldots,A_{10}$ $B_1,B_2,\ldots,B_{10}$	=	coefficients
f,g,h,j,k,m	=	complex constants
F	=	applied force in static spring constant measurement
$I_1,I_2,\ldots,I_7$	=	centroidal moments of inertia of $m_1,m_2,\ldots,m_7$, respectively
K_1,K_2,K_3	=	spring constants
ℓ	$\equiv$	$\ell_1 \approx \ell_2$
ℓ_3	=	distance from pivot point to line of action of F in static spring constant measurement
$m_1,m_2,\ldots,m_7$	=	lumped masses representing the mathematical model of the physical system
n	=	number of cycles of free oscillation
p	=	dynamic pressure at the nozzle of the jet
P	=	force on the attachment due to the impact of the fluid jet
P_b	=	critical load for divergence
P_d	=	critical load for damped flutter

P_x, P_y	=	components of P
P_*	=	critical load for undamped flutter
q, r, s	=	complex constants
R	=	amplitude ratio
S_1, S_2	=	proportionality constants
u, v, w	=	complex constants
α	=	nonconservativeness parameter
ϵ	=	$\epsilon_1 / \epsilon_2 \ell^2$
ϵ_1	=	torsional damping constant associated with each hinge
ϵ_2	=	linear damping constant associated with viscous damping on the attachment
τ	=	period of oscillations
φ_1, φ_2	=	angular displacements of Bars I and II, respectively
$\varphi_{10}, \varphi_{20}$	=	initial values of φ_1 and φ_2, respectively
$\bar{\varphi}_1, \bar{\varphi}_2$	=	$\varphi_1 - \varphi_{10}$ and $\varphi_2 - \varphi_{20}$, respectively
Φ_1, Φ_2	=	undetermined amplitudes of assumed solution to differential equations of motion
ω	=	angular frequency of system oscillations
$\omega_1, \omega_2, \omega_3$	=	natural frequencies in spring constant determination

1. INTRODUCTION

Theoretical studies of stability of elastic systems subjected to nonconservative (also termed circulatory) forces have revealed a number of interesting phenomena. An account of the development in this field is given by Herrmann in a survey article [1]*. In the majority of these studies, however, the forces are introduced rather artificially and without any reference as to their possible physical origin. In a recent report [2], a series of structural models embodying the features that are peculiar to the behavior of such nonconservative systems is described qualitatively. It is the aim of the present study to report quantitative results which were obtained in the course of experimentation with one of the models discussed in [2], and compare the results with the theoretical predictions.

The mathematical model of the physical system considered here may be called Reut's problem. It consists of a cantilever with a rigid plate at its free end, which is normal to the axis. It is subjected to a force, acting on the plate, which is always collinear with the undeformed axis of the cantilever, see Fig. 1. Bolotin [3] reports that this problem was first posed by Reut in 1939 and solved by B. L. Nikolai in the same year. In this context, Bolotin suggests that the force in Reut's problem may be realized by an impinging jet of absolutely inelastic particles, since the kinetic energy of the particles is completely absorbed upon impact. To the authors' knowledge no attempt was ever made to follow up these suggestions, or to realize Reut's problem in any other way. Bolotin also suggests that the pressure from a jet of liquid or gas may induce such a force when the

---

* Numbers in brackets designate References at end of paper.

inclination of the force, as the bar deforms, is neglected.

In an attempt to construct models based on these ideas, the authors discovered that by covering the plate with screens of certain mesh sizes a problem very close to the Reut's one may be realized. The resultant force, in this case, has an inclination which can be controlled by a suitable arrangement of screens of various mesh sizes; the point of application of the resultant force, however, always lies on the axis of the undeformed cantilever. When this force stays normal to the end plate, the system loses stability by divergence (attainment of another equilibrium state); the force is conservative. On the other hand, if the force stays collinear with the undeformed axis of the bar, the loss of stability occurs by flutter (oscillations with increasing amplitudes); the force is nonconservative. By controlling the inclination of the force, various degrees of nonconservativeness may be attained.

The experimental results are obtained using a system with two degrees of freedom, rather than a continuous cantilever. The applied force is induced by an impinging air jet. The degree of nonconservativeness is controlled by employing suitable end attachments, resulting in either divergent- or flutter-type motions of the system. Also, the effect of viscous damping forces is investigated. It is found that the experimentally obtained flutter-load corresponds rather closely to the theoretical prediction when small dissipative forces are included; this confirms the earlier findings that small damping forces may have a destabilizing effect [3-13].

2. DESCRIPTION OF MODEL AND SUPPORTING EQUIPMENT

The model consists of two like rigid rods (Fig. 2). One rod is elastically hinged to a fixed base while the other is elastically hinged to the first rod and free at the other end. The system is constrained to move in a horizontal plane, being supported by long, light wires. Various rigid attachments can be placed at the free end of the second rod. The attachment consists basically of a rigid flat plate covered with a combination of screens of various mesh sizes and sandpapers of various degrees of coarseness. This attachment is rigidly fixed and mounted normal to the axis of the second rod. In the absence of any disturbance, the system is in equilibrium when the two rods are collinear (undisturbed configuration).

A fixed nozzle is placed along the equilibrium axis of the system, one inch away from the attachment, and an air jet is made to impinge upon the attachment. The flow rate can be varied by means of a valve. The dynamic pressure at the nozzle corresponding to a given flow rate can be read from a dial gage.

It is observed that as the flow rate, and hence the force on the attachment, is increased and passes a certain (critical) value, the system does not remain in the undisturbed configuration. Stability is lost by either flutter (oscillations with increasing amplitudes) or by divergence (buckling (the attainment of another equilibrium state)), depending on the nature of the attachment used. If the attachment is a flat plate with a smooth surface (a flat sheet of aluminum) facing the air jet, then the loss of stability occurs by divergence. By contrast, flutter-type motion is observed if the attachment is a plate with screens of certain mesh sizes placed on the

surface that faces the impinging fluid. The sequence of photographs in Fig. 3 illustrates the flutter-type motion, while Fig. 4 depicts a buckled state (divergence). Figure 5 and Table 1 present the numerical values for all the relevant properties of the system.

The supporting equipment consists of a calibrating system which is used to correlate the dynamic pressure, hence the flow rate, with the actual force which acts on the system. Three square steel plates are placed horizontally one above the other, and are separated and supported by sets of steel leaf springs. The steel leaf springs connecting the two lower plates permit displacement in only one direction, while those connecting the upper two plates permit displacement only in the perpendicular direction. Two stages are thus formed. The displacement of each stage is, with a high degree of accuracy, proportional to the component of the force which acts along the direction of the displacement. With the aid of a pair of strain gages attached to the steel leaf springs, and using a compensating network, readings can be taken which are proportional to the respective displacements of each stage. In this manner, strain gage readings can be related to the magnitude of the force acting on the system.

The supporting equipment described above is used to find the direction and the magnitude of the force on the attachment when the dynamic pressure ot the impinging air jet at the nozzle is known. The attachment is mounted on the top plate of the supporting stages and then subjected to the air jet at a given angle of incidence, see Fig. 6. The magnitude and the direction of the resultant force corresponding to a given angle of incidence and for a given dynamic pressure are thus obtained experimentally.

3. THEORY

As was pointed out in Section 1, the problem of a cantilever with a rigid cross-plate at its free end and subjected to a force which is always directed along the initial, undeformed axis of the cantilever, was first posed by Reut in 1939. It is essential to note that the applied force in Reut's problem is not attached to a material point of the system, but rather to a line in space. In structural mechanics, boundary value problems are commonly posed for surface tractions which are connected to the material points upon which they act. As a result, the difference between the displacements of the material points and of the points of application of the forces disappears.

In the present problem, the force is induced by the action of an air jet upon the end plate. It may be assumed that such an action is equivalent to a resultant force whose point of application lies always on the axis of the undeformed system, that is, along the direction of the flow. This force continuously disengages from the material point on which it is instantaneously acting. This force is conservative only if it stays normal to the end plate as the system deforms. In the subsequent analysis, we will denote this force by **P** and the angle by which it rotates as the system deforms, by $\alpha\varphi_2$.

We consider small lateral motions of the system as shown in Fig. 5. The rigid bar, designated by I, is connected to the support by a rotational spring of stiffness K_1 and carries at its other end a rotational spring of stiffness K_2 to which is attached another rigid rod, designated as II. In addition, rods I and II are connected to two linear coil springs as shown in

Fig. 5. Since the displacement of the spring connected to bar I is not coupled with the motion of the bar II, the stiffness K_1 properly accounts for the effect of this spring. The spring connected to bar II is located at a distance d_2 from the center of the middle joint and has stiffness K_3.

The inertial properties are represented by seven masses m_j, $j = 1,2,...7$, and seven centroidal moments of inertia I_j, $j = 1,2,...7$. The mass of the end rotational spring is denoted by m_1, and that of the rod I is denoted by m_2. The central rotational spring has in effect two masses m_3 and m_4 which are attached to the rods I and II, respectively. The mass of the rod II is m_5, and m_6 is that of the collar which fits the attachment having mass m_7.

The distance between the centers of the end and the middle rotational springs is denoted by ℓ_1, while the mass m_7 is at a distance ℓ_2 from the center of the middle joint. The dimensions a_1, b_1 and c_1 are the distances from the center of the end joint to masses m_1, m_2 and m_3, respectively, while a_2, b_2 and c_2 designate the respective distances of m_4, m_5 and m_6 from the center of the middle joint.

The two rotational springs were made of high tempered spring steel with identical geometry and, therefore, they have small damping with, plausibly, the same damping constant ϵ_1. Since the attachment has a large surface area which moves relative to the impinging air jet, an external linear damping with constant ϵ_2 appears to be a reasonable representation of the corresponding damping mechanism.

The magnitude of the force due to the impinging air jet is P, the direction of which encloses an angle $\alpha\varphi_2$ with the undeformed axis. α is assumed to be a constant which will be determined experimentally with the

help of the auxiliary equipment as described in Section 4. φ_1 and φ_2 are the respective rotations of bars I and II from the initial straight position.

The following equations of motion are obtained by employing D'Alembert's principle:

$$\begin{aligned} A_{11}\ddot{\varphi}_1 + A_{12}\ddot{\varphi}_2 + B_{11}\dot{\varphi}_1 + B_{12}\dot{\varphi}_2 + (C_{11} - P\ell_1)\varphi_1 + (C_{12} + P\ell_1\alpha)\varphi_2 = 0 \\ A_{21}\ddot{\varphi}_1 + A_{22}\ddot{\varphi}_2 + B_{21}\dot{\varphi}_1 + B_{22}\dot{\varphi}_2 + (C_{21} + P\ell_1)\varphi_1 + (C_{22} + P\ell_2\alpha)\varphi_2 = 0 \end{aligned} \tag{1}$$

where

$$\begin{aligned} A_{11} &= (m_4 + m_5 + m_6 + m_7)\ell_1^2 + m_1a_1^2 + m_2b_1^2 + m_3c_1^2 + I_1 + I_2 + I_3 \\ A_{12} &= A_{21} = (m_4a_2 + m_5b_2 + m_6c_2 + m_7\ell_2)\ell_1 \\ A_{22} &= m_4a_2^2 + m_5b_2^2 + m_6c_2^2 + m_7\ell_2^2 + I_4 + I_5 + I_6 + I_7 \\ B_{11} &= \epsilon_2\ell_1^2 + 2\epsilon_1 \\ B_{12} &= B_{21} = \epsilon_2\ell_1\ell_2 - \epsilon_1 \\ B_{22} &= \epsilon_2\ell_2^2 + \epsilon_1 \\ C_{11} &= K_1 + K_2 + K_3\ell_1^2 \\ C_{12} &= C_{21} = -K_2 + K_3\ell_1d_2 \\ C_{22} &= K_2 + K_3d_2^2 \end{aligned} \tag{2}$$

A. Undamped System - Flutter.

Consider first the undamped case, i.e., let $\epsilon_1 = \epsilon_2 \equiv 0$. Then $B_{ij} = 0$. Assuming solutions of the form

$$\begin{aligned} \varphi_1 &= \Phi_1 e^{i\omega t} \\ \varphi_2 &= \Phi_2 e^{i\omega t}, \end{aligned} \tag{3}$$

where $i = \sqrt{-1}$, Φ_1 and Φ_2 are undetermined amplitudes, ω is an undetermined frequency and t is the time variable, the associated frequency equation is

$$a\omega^4 + b\omega^2 + c = 0, \tag{4}$$

where

$$\begin{aligned} a &= A_{11}A_{22} - A_{12}^2 \\ b &= 2A_{12}C_{12} + A_{12}P\ell_1(1+\alpha) - A_{11}P\ell_2\alpha - A_{11}C_{22} - A_{22}C_{11} + A_{22}P\ell_1 \\ c &= C_{11}P\ell_2\alpha - P^2\ell_1\alpha(\ell_1 + \ell_2) - C_{12}P\ell_1\alpha - C_{12}P\ell_1 + C_{11}C_{22} - C_{12}^2 - C_{22}P\ell_1 \end{aligned} \tag{5}$$

Flutter occurs if ω is complex with a negative imaginary part. The threshold (critical) value of P, called P_*, is obtained by setting

$$b^2 - 4ac = 0 \tag{6}$$

and is

$$P_{*_{1,2}} = \frac{2hk - fg}{f^2 - 4hj} \pm \frac{2}{f^2 - 4hj}\sqrt{h^2k^2 - hkfg - 4h^2jm + hjg^2 + hmf^2} \tag{7}$$

where

$$\begin{aligned} f &= A_{12}\ell_1(1+\alpha) - A_{11}\ell_2\alpha + A_{22}\ell_1 \\ g &= 2A_{12}C_{12} - A_{11}C_{22} - A_{22}C_{11} \\ h &= A_{11}A_{22} - A_{12}^2 \\ j &= -\ell_1\alpha(\ell_1 + \ell_2) \\ k &= C_{11}\ell_2\alpha - C_{12}\ell_1\alpha - C_{12}\ell_1 - C_{22}\ell_1 \\ m &= C_{11}C_{22} - C_{12}^2 \end{aligned} \tag{8}$$

As the value of P is increased, flutter will occur when P becomes equal to the lower value of P_*. Note that P_* is a function of α through Eqs. (8).

P_* exists only when the argument of the square root in Eq. (7) is non-negative.

B. Damped System - Flutter.

Using an assumed solution of the form (3) in Eqs. (1) results in the following determinant which is set equal to zero for a nontrivial solution:

$$\begin{vmatrix} -\omega^2 A_{11} + C_{11} - P\ell_1 + i\omega B_{11} & -\omega^2 A_{12} + P\ell_1\alpha + C_{12} + i\omega B_{12} \\ -\omega^2 A_{12} + C_{12} + P\ell_1 + i\omega B_{12} & -\omega^2 A_{22} + P\ell_2\alpha + C_{22} + i\omega B_{22} \end{vmatrix} = 0 \tag{9}$$

If we neglect the product of ϵ_1 and ϵ_2 in the expansion of (9), we obtain two equations by separating the real and imaginary parts. The first equation is the same as Eq. (4). The equation resulting from the imaginary part yields the following relation:

$$\omega^2 = \frac{B_{11}(P\ell_2\alpha + C_{22}) + B_{22}(C_{11} - P\ell_1) - B_{12}[P\ell_1(1+\alpha) + 2C_{12}]}{A_{22}B_{11} + A_{11}B_{22} - 2A_{12}B_{12}} \tag{10}$$

Substituting ω^2 from Eq. (10) into Eq. (4) and denoting by P_d the threshold values of P for this case, results in

$$P_{d_{1,2}} = -\frac{u}{2w} \pm \frac{1}{2w}\sqrt{u^2 - 4wv}\ , \tag{11}$$

where

$$\begin{aligned} u &= \frac{2hqr}{s^2} + \frac{qg + fr}{s} + k \\ v &= \frac{hr^2}{s^2} + \frac{gr^2}{s} + m \\ w &= \frac{hq^2}{s^2} + \frac{fq}{s} + j \end{aligned} \tag{12}$$

and

$$q = \ell(3\epsilon\alpha - 2)$$

$$r = (1 + 2\epsilon)C_{22} + (1 + \epsilon)C_{11} - 2C_{12}(1 - \epsilon) \tag{13}$$

$$s = (1 + 2\epsilon)A_{22} + (1 + \epsilon)A_{11} - 2A_{12}(1 - \epsilon),$$

where

$$\epsilon \equiv \epsilon_1/\epsilon_2\ell^2 \quad \text{and} \quad \ell \equiv \ell_1 \approx \ell_2. \tag{14}$$

Thus the critical force depends not only on α, but also on ϵ, essentially the ratio of the damping coefficients. The critical force is the lower of the two values of P_d and it exists only when the argument of the square root in Eq. (11) is non-negative.

C. Divergence.

For divergence, or buckling, ω is set equal to zero in Eq. (4). The condition is then

$$c = 0. \tag{15}$$

Denoting the value of P at which this occurs by P_b, we have

$$P_{b_{1,2}} = -\frac{k}{2j} \pm \frac{1}{2j}\sqrt{k^2 - 4jm}\ , \tag{16}$$

where j, k and m are defined by Eqs. (8).

As are P_* and P_d, P_b is also a function of α, but it is independent of the mass distribution. P_b exists only if $k^2 - 4jm \geq 0$.

D. Results.

With the system parameters given, including the spring constants, which are determined experimentally (see Section 4), Eqs. (7), (11) and (16) must be solved for P for each specified value of α. This repetitious task was performed with the aid of a CDC 3400 computer in use at the Vogelback Computing Center of Northwestern University.

As can be seen in Fig. 5, for $\alpha = 0$, the force **P** is always directed along the equilibrium line, i.e., the line defined by $\varphi_1 = \varphi_2 = 0$. When $\alpha = 1$, the force is always perpendicular to the surface of the attachment. As discussed earlier, in the former case the force is nonconservative, while in the latter it is conservative. It turns out that with the present set-up, experimentally realizable α are in the range $0.23 \leq \alpha \leq 0.91$.

Unfortunately, mechanical failure of the joints occurred during the advanced stage of experimental measurements and, consequently, when the model was reassembled, the spring constants K_1, K_2 and K_3 changed. Thus it became necessary to designate the previous model by system **I** and the re-assembled model by system **II**. With due respect to the difference in system parameters, stability curves, **P** vs. α, are shown in Figs. 12 and 13.

4. EXPERIMENTAL PROCEDURE AND RESULTS

A. Correlation of the Force with Air Pressure and Determination of α.

To find the magnitude and the direction of the force acting on the attachment due to a given air flow rate, the supporting equipment described in Section 2 is used.

The nozzle assembly is detached from the model and mounted adjacent to the calibrating device (Fig. 6), parallel to the direction of motion of one of the stages. The rigid attachment is separated from the model and mounted on a special bracket on the top plate of the calibrating stages. This bracket may be rotated so that the angle between a normal to the attachment and the center line of the nozzle, namely, φ_2, may be varied. Markings are provided for $\varphi_2 = 0, 5, 10, 15, 20, 25$ and 30°.

The first step is to find a relation between the displacement of the stages and the force applied to the top plate. This is done by applying known forces along the deflections of each stage and noting the strain gage readings. If the direction parallel to the nozzle is designated by x and the perpendicular direction by y, relations of the form

$$\begin{aligned} P_x &= S_1 \Delta e_x \\ P_y &= S_2 \Delta e_y \end{aligned} \tag{17}$$

may be written. P_x and P_y are the forces, and Δe_x and Δe_y are the differences in strain gage readings between no load and full load, for the x- and y-directions, respectively. S_1 and S_2 are the proportionality constants.

The next step is to correlate the force, P, with the air pressure, p. From the free-body diagram of the attachment mounted on the calibrating system (Fig. 7), the following relations are obtained:

$$P_x(p) = P(p) \cos \alpha(p)\varphi_2$$
$$P_y(p) = P(p) \sin \alpha(p)\varphi_2, \tag{18}$$

where the force P has been split into its components P_x and P_y, which are functions of the pressure, p. The parameter α is assumed to be a function of p also. From Eqs. (18) we can write

$$\arctan \left[\frac{P_y}{P_x} (p) \right] = \alpha(p)\varphi_2 \tag{19}$$

For a given attachment and angle φ_2, strain gage readings are taken for a set of pressures. These in turn yield the forces P_x and P_y corresponding to each pressure. The angle of incidence, φ_2, is then varied from 0° to 30° in 5° increments and for each value of φ_2 an average value for P_y/P_x is obtained over a range of pressures p. It turns out experimentally that P_x and P_y are linear functions of p, as one would expect, and thus the ratio P_y/P_x is independent of p. This means that α must be independent of p because of Eq. (19). If arctan P_y/P_x is plotted vs. φ_2, the result is (very nearly) a straight line and, therefore, the slope may be interpreted as α in Eq. (19). α is a constant for a given attachment.

The critical force is read, or interpolated, as the value of P_x at $\varphi_2 = 0$ corresponding to the critical value of pressure. For small φ_2, $P \approx P_x$; this is within the scope of the linearized theory.

In this manner, the value of α is obtained experimentally for each attachment.

B. Determination of Stiffnesses.

(a) Dynamic Method. The spring constants K_1, K_2 and K_3 may be determined experimentally by a simple dynamic analysis of various motions

of the system.

The spring constant K_1 associated with the end joint and the linear spring attached to bar I may be evaluated by locking the middle joint so that the two bars move as a rigid unit (Fig. 8). The linearized equation of motion then is:

$$K_1\varphi_1 + \left[m_1a_1^2 + m_2b_2^2 + m_3c_1^2 + m_4(\ell_1 + a_2)^2 + m_5(\ell_1 + b_2)^2 + m_6(\ell_1 + c_2)^2 + m_7(\ell_1 + \ell_2)^2 + I_1 + I_2 + I_3 + I_4 + I_5 + I_6 + I_7\right]\ddot{\varphi}_1 = 0, \tag{20}$$

from which

$$\omega_1^2 = K_1 \Big/ \left[m_1a_1^2 + m_2b_2^2 + m_3c_1^2 + m_4(\ell_1 + a_2)^2 + m_5(\ell_1 + b_2)^2 + m_6(\ell_1 + c_2)^2 + m_7(\ell_1 + \ell_2)^2 + I_1 + I_2 + I_3 + I_4 + I_5 + I_6 + I_7\right]$$

or

$$K_1 = \omega_1^2\left[m_1a_1^2 + m_2b_2^2 + m_3c_1^2 + m_4(\ell_1 + a_2)^2 + m_5(\ell_1 + b_2)^2 + m_6(\ell_1 + c_2)^2 + m_7(\ell_1 + \ell_2)^2 + I_1 + I_2 + I_3 + I_4 + I_5 + I_6 + I_7\right], \tag{21}$$

where ω_1 denotes the measured natural frequency of the system.

In a similar manner, the spring constant K_2 of the middle joint may be determined by locking the end joint, removing the linear spring attached to bar II and allowing the system to oscillate freely (Fig. 9). Then K_2 is given by

$$K_2 = \omega_2^2\left[m_4a_2^2 + m_5b_2^2 + m_6c_2^2 + m_7\ell_2^2 + I_4 + I_5 + I_6 + I_7\right], \tag{22}$$

where ω_2 is the measured natural frequency.

Spring constant K_3 can be found if K_2 is known. When the linear spring is attached to bar II, the equation of motion becomes

$$K_2\varphi_2 + \left[m_4a_2^2 + m_5b_2^2 + m_6c_2^2 + m_7\ell_2^2 + I_4 + I_5 + I_6 + I_7\right]\ddot{\varphi}_2 + K_3d_2\varphi_2 = 0, \qquad (23)$$

whence

$$K_3 = \frac{\left[m_4a_2^2 + m_5b_2^2 + m_6c_2^2 + m_7\ell_2^2 + I_4 + I_5 + I_6 + I_7\right]\omega_3^2 - K_2}{d_2^2}, \qquad (24)$$

where ω_3 is the measured natural frequency.

(b) Static Method. An alternate procedure for determining the spring constants is to use a static method whereby forces are applied and the resulting deflections measured.

To evaluate K_1, the middle joint is locked so that bars I and II move as a unit. The linear spring on bar II is detached. At a known point along the bar a force is applied and the lateral deflection of that point is measured (Fig. 10). From equilibrium

$$K_1\varphi_1 = \ell_3F, \qquad (25)$$

but $\varphi_1 = d/\ell_3$, and thus

$$K_1 = \ell_3^2F/d, \qquad (26)$$

where F is the applied force, ℓ_3 is the distance from the center of the end joint to the line of action of the force, and d is the deflection. Equations (25) and (26) are valid for small deflections only.

In a similar manner, K_2 may be determined by fixing bar I in its equilibrium position, applying a force, and measuring the resulting deflection (Fig. 11). The linear spring on bar II should remain detached. The result is identical to Eq. (26) except that ℓ_3 is interpreted as the distance from the center of the middle joint to the point of application of the force.

The remaining spring constant, K_3, may be determined by using the same

set-up as above but leaving the linear spring attached to bar II. Then, from equilibrium

$$K_3 = \left[\frac{F\ell_3^2}{d} - K_2\right] \Big/ d_2^2 \ , \tag{27}$$

where ℓ_3, d and F are interpreted as in the determination of K_2 above, and d_2 is the distance from the line of action of the linear spring to the center of the middle joint.

Theoretically, these two methods should yield identical results. Experimentally, the results of the two methods differed slightly (see Table 1). The static measurement is to be preferred because the dynamic method depends upon the square of experimentally measured frequencies which are not known with great accuracy.

C. Summary and Results.

The basic steps in the experimental procedure are as follows: First, choose an attachment and mount it on the model. Raise the air pressure slowly from zero and note the critical pressure at which the system starts exhibiting amplified oscillations (flutter) or shows a static loss of stability (buckling). The supporting equipment is then used to find α and to find the force P corresponding to the critical pressure p. The spring constants are then determined experimentally for use in the theoretical analysis (Section 3).

When choosing attachments, it is desirable that they all be of about the same weight and that a wide range of α be covered more or less uniformly. A wide variety of screens and sandpapers were weighed and combinations were chosen that met these requirements. The values of α which were experimentally realized lie in the range 0.238 to 0.913, the latter being for

an attachment consisting of a smooth flat plate.

In Figs. 12 and 13, the experimental results are shown together with the theoretical curves. As was mentioned in Section 3, two systems had to be considered because of a mechanical failure of the joints. For each experimental run a point of instability is drawn on the diagram at the corresponding α and P. A $\odot$ is used for a flutter point, while $\otimes$ is used to denote divergence. The measurements are labeled 1 through 8 for System I and 1 through 12 for System II.

Table 2 summarizes the experimental and theoretical results and provides a comparison between these results.

5. DISCUSSION OF RESULTS, CONCLUSIONS AND RECOMMENDATIONS

The results of this study are summarized in Figs. 12 and 13 and in Table 2. It is noted that the experimentally determined critical points lie somewhat below the theoretical stability curves for undamped flutter and divergence. In the discussion which follows, the possible reasons for this discrepancy are explored.

One of the primary reasons for the discrepancy between the theoretical stability curve for undamped flutter and the experimentally observed points of flutter appears to lie in the fact that damping is present in the physical system. The damping mechanism assumed in the analysis has already been discussed. Stability curves for flutter with small damping taken into account are shown in Figs. 12 and 13 for several values of the damping ratio ϵ. It is seen from these figures that in the presence of damping the theoretical stability curves come to pass very near the experimental points. It is shown in Appendix A that the assumed values of ϵ are realistic. No attempt is made here to determine ϵ with a high degree of accuracy since the assumed damping mechanism, while reasonable, is chosen mostly for its simplicity and it is doubtful that it represents completely the actual damping in the system.

The results presented indicate that damping has a destabilizing effect on the system and that the presence of damping extends the flutter region to higher values of α. Also, the lower values of the damping ratio are associated with lower values of flutter loads and a wider flutter range. This confirms results shown previously in [10].

The theoretical curves bounding the regions of flutter (with and

without damping) and divergence were found to be rather insensitive to small changes in system parameters, as indicated in Table 1, with the possible exception of the spring constants. The dynamic measurement of the spring constants provides another possible source for the discrepancy since the calculation depends on the square of a measured quantity, i.e., the frequency of free oscillations. But, the spring constants were determined also using the static method previously described. Difficulties may arise here, however, in measuring the applied force by means of hanging weights on a light string which passes over an air bearing.

Since the two methods of measuring the spring constants gave somewhat different results (Table 1), it was decided to investigate the effect of a 5% difference in either K_1, K_2 or K_3. A computer program was written in which each calculated spring constant was subjected to a ± 5% uncertainty. If an envelope is drawn about the nine curves thus obtained, the effect is roughly to give a maximum error of ± 6 gm (or ± 4 - 10%). No other system parameter (Table 1) is subject to an error approaching 5%, except possibly the moments of inertia, but these are insignificant when compared to the mass-times-distance-squared terms to which they are added.

The observed discrepancy between the theoretical curve for divergence and the experimental points may be due also, in part, to the uncertainty in the values of the spring constants, but the major cause of error seems to lie in the possibility of initial imperfections and nonlinear effects.

Since the physical model is not an ideal linear system free of imperfections, there is no single, sharply defined divergence load. An arbitrary criterion of the load required for a one-inch deflection of the middle joint was used as the condition for divergence. By this definition, the

experimental points of divergence were somewhat below (15-25%) the divergence curves obtained from the linear analysis (Figs. 12, 13 and Table 2). In an attempt to explain this discrepancy it seems advisable to investigate the nonlinear divergence theory as well as the effects of initial imperfections. This is discussed in detail in Appendix B for $\alpha = 0.717$ (run 11).

The results of this investigation are shown in Fig. 14, with a detailed description of the curves given in Appendix B. It is noted that the postulated criterion for divergence gives very nearly the same load for both the linear (curve A) and the nonlinear (curve B) cases, and thus the theoretical divergence curves given in Figs. 12 and 13 actually represent the divergence loads for the nonlinear theory in conjunction with the adopted criterion.

The strong effect of imperfections on the divergence load is discussed in Appendix B. Initial imperfections in the amount $\varphi_{10} = 0.01$, $\varphi_{20} = -0.01$, as shown in curve D, are indeed reasonable for this model. This corresponds to a no-load deflection of about 0.1 inch at the middle joint. This small imperfection lowers the theoretical divergence load by about 15%.

Curve F is the experimental force-deflection curve for run 11. Note that the shape of the curve differs somewhat from the theoretical curves shown. It should be pointed out that the points used to draw this curve are rather difficult to obtain since holding the air pressure constant to obtain a deflection reading does not prevent the motion of the model. Since the run of the curve F is somewhat different from the other curves, the likelihood exists that other sources for the discrepancy may be present. It may be appropriate to mention here that it has been noted repeatedly in the past that structural systems buckle at loads below those theoretically expected.

To provide better insight into the discrepancy under discussion, the experimental procedure was also scrutinized. The method of correlating the air pressure as read on the dial gage, to the actual force on the attachment, was studied with the conclusion that no appreciable error could be introduced.

As is pointed out in [1], more experimental work is needed in the area of systems subjected to nonconservative forces. The present study is thus expected to be merely a first contribution to quantitative experimentation in this special field of stability of mechanical systems.

APPENDIX A

Approximation to the Damping Ratio

If the end joint is locked and the linear spring attached to bar II is removed, the equation of motion of bar II under the action of a force **P** from the nozzle becomes

$$\left[m_4a_2^2 + m_5b_2^2 + m_6c_2^2 + m_7\ell_2^2 + I_4 + I_5 + I_6 + I_7\right]\ddot{\varphi} + \left[\epsilon_2\ell_2^2 + \epsilon_1\right]\dot{\varphi}_2 + \left[K_2 + P\alpha\ell_2\right]\varphi_2 = 0. \tag{A.1}$$

This may be solved for φ_2 by elementary means to yield, for small damping

$$\varphi_2 = Ce^{-At}\cos\sqrt{B^2 - A^2}\,t, \tag{A.2}$$

where

$$\begin{aligned} A &= \left(\epsilon_2\ell_2^2 + \epsilon_1\right) \Big/ D \\ B^2 &= (K_2 + P\alpha\ell_2)/D \\ C &= \text{a constant} \\ D &= m_4a_2^2 + m_5b_2^2 + m_6c_2^2 + m_7\ell_2^2 + I_4 + I_5 + I_6 + I_7. \end{aligned} \tag{A.3}$$

The ratio of any two amplitudes is given by

$$R = a_n/a_1 = e^{-An\tau} \tag{A.4}$$

or

$$A = -\log R/n\tau, \tag{A.5}$$

where a_n is the nth amplitude, a_1 is the initial amplitude and τ is the period. This provides one relation in the unknown quantities ϵ_1 and ϵ_2.

The damping on the attachment is assumed to be due to the drag on the attachment as it moves through the ambient air. This drag can be eliminated

if the attachment is removed, but this would alter D in Eqs. (A.3). If the attachment is replaced with an object of the same mass and moment of inertia, but with significantly less surface area, thus creating much less drag, an equation involving ϵ_1 only would be obtained. Fortunately, $I_7 \ll m_7 \ell_2^2$, so the latter requirement is unnecessary. The attachment was thus replaced with a piece of lead of mass m_7. Then

$$A^* = \epsilon_1 / D, \tag{A.6}$$

where the asterisk denotes the fact that the dummy mass m_7 is used.

Equation (A.6) and the first of Eqs. (A.3) then give two equations in the two unknowns ϵ_1 and ϵ_2. The procedure then is to measure the frequency of free oscillations, the initial amplitude and the amplitude after n cycles, for bar II with the attachment in place, and repeat the procedure with the dummy mass.

The damping ratio ϵ is given by

$$\epsilon = \frac{\epsilon_1}{\epsilon_2 \ell_2^2} = \frac{A^* D}{AD - \epsilon_1} = \frac{A^*}{A - A^*} . \tag{A.7}$$

A^* and A are found from Eq. (A.5), with R, n and τ being obtained experimentally.

Using experimental measurements,

$$\epsilon = \frac{A^*}{A - A^*} = - \frac{\log R^*}{n\tau^*} \Big/ \left(- \frac{\log R}{n\tau} - \frac{\log R^*}{n\tau} \right) = - \frac{0.1055}{0.0999 - 0.1055} = 18.8,$$

where the asterisk again refers to measurements taken with the dummy mass in place.

Of course, this result is approximate since there is some damping on the replacement mass and also because ϵ is very sensitive to small changes

in the R's, which are, in turn, based on measured amplitudes which are subject to considerable error. However, this result does support the choice of $\epsilon = 5.0$ as being of the correct order of magnitude.

APPENDIX B

Nonlinear Divergence Analysis

The equations of motion, assuming φ_1 and φ_2 are not small, neglecting inertial effects, thereby restricting the equations to use for divergence analysis, and allowing for imperfections by assuming that the equilibrium configuration is not a straight line, are:

$$\begin{aligned} &K_1\bar{\varphi}_1 - K_2(\bar{\varphi}_2 - \bar{\varphi}_1) - P\ell_1\cos\alpha\varphi_2\sin\varphi_1 + K_3\ell_1(\ell_1\sin\bar{\varphi}_1 + d_2\sin\bar{\varphi}_2)\cos\bar{\varphi}_1 \\ &\qquad + P\ell_1\sin\alpha\varphi_2\cos\varphi_1 = 0 \\ &K_2(\bar{\varphi}_2 - \bar{\varphi}_1) + P\sin\alpha\varphi_2[\ell_2\cos\varphi_2 + \tan\varphi_2(\ell_1\sin\varphi_1 + \ell_2\sin\varphi_2)] \\ &\qquad + P\ell_1\cos\alpha\varphi_2\sin\varphi_1 + K_3d_2(\ell_1\sin\bar{\varphi}_1 + d_2\sin\bar{\varphi}_2)\cos\bar{\varphi}_2 = 0, \end{aligned} \tag{B.1}$$

where $\bar{\varphi}_1 = \varphi_1 - \varphi_{10}$, $\bar{\varphi}_2 = \varphi_2 - \varphi_{20}$, and φ_{10} and φ_{20} are the no-load values of φ_1 and φ_2, respectively.

Restricting the magnitude of φ_1 and φ_2 by setting

$$\begin{aligned} \sin\varphi_1 &= \varphi_1 - \varphi_1^3/6 \\ \cos\alpha\varphi_2 &= 1 - (\alpha\varphi_2)^2/2 , \end{aligned} \tag{B.2}$$

the equations may be written as polynomials of the form

$$\begin{aligned} &A_1\varphi_1^3 + A_2\varphi_2^3 + A_3\varphi_1\varphi_2^2 + A_4\varphi_1^2\varphi_2 + A_5\varphi_1^2 + A_6\varphi_2^2 + A_7\varphi_1\varphi_2 \\ &\qquad + A_8\varphi_1 + A_9\varphi_2 + A_{10} = 0 \\ &B_1\varphi_1^3 + B_2\varphi_2^3 + B_3\varphi_1\varphi_2^2 + B_4\varphi_1^2\varphi_2 + B_5\varphi_1^2 + B_6\varphi_2^2 + B_7\varphi_1\varphi_2 \\ &\qquad + B_8\varphi_1 + B_9\varphi_2 + B_{10} = 0. \end{aligned} \tag{B.3}$$

A computer program was written to solve these two third-degree algebraic equations simultaneously for various values of **P**, φ_{10} and φ_{20}. The

results are given in Fig. 14 for $\alpha = 0.717$ (run 11) in the form **P** vs. φ_1. The variation of φ_2 with **P** is essentially similar. The vertical dotted line represents the angle φ_1 corresponding to one-inch deflection of the middle joint, which is the buckling criterion used in this study.

Curve **A** represents the linear case for $\varphi_{10} = \varphi_{20} = 0$. No deflection occurs until the buckling load is reached. Curve **B** represents the imperfection-free nonlinear case where the approximations (B.2) are used. The buckling loads predicted by curves **A** and **B** are rather close.

Curves **C**, **D** and **E** are drawn for the values of φ_{10} and φ_{20} indicated. Note that the buckling loads, as determined by the intersection of the response curves with the dotted vertical line, depend significantly on the magnitudes of φ_{10} and φ_{20}.

Curve **F** is the experimental response curve for the model with the attachment used for run 11 ($\alpha = 0.717$) in place.

REFERENCES

[1] Herrmann, G., "Stability of Equilibrium of Elastic Systems Subjected to Nonconservative Forces," AMR 20, 1967, pp. 103-108.

[2] Herrmann, G., S. Nemat-Nasser and S. N. Prasad, "Models Demonstrating Instability of Nonconservative Mechanical Systems," Northwestern University Structural Mechanics Laboratory Tech. Report No. 66-4, June 1966.

[3] Bolotin, V. V., Nonconservative Problems of the Theory of Elastic Stability, Moscow, 1961; English translation published by Pergamon Press, Inc., New York, N.Y., 1963.

[4] Ziegler, H., "Stabilitätsprobleme bei geraden Stäben und wellen," ZAMP 2, 1951, pp. 265-289.

[5] Ziegler, H., "Knickungerader Stabeunter Torsion," ZAMP 3, 1952, pp. 96-119.

[6] Ziegler, H., "Die Stabilitätskriterien der Elastomechanik," Ingenieur Archiv 20, 1952, pp. 49-56.

[7] Ziegler, H., "Linear Elastic Stability," ZAMP 4, 1953, pp. 89-184.

[8] Ziegler, H., "On the Concept of Elastic Stability," Advances in Applied Mechanics, 4, edited by H. L. Dryden and T. von Karman, Academic Press, Inc., New York, N.Y., 1956, pp. 351-403.

[9] Herrmann, G. and I. C. Jong, "On the Destabilizing Effect of Damping in Nonconservative Elastic Systems," J. Appl. Mech. 32, 1965, pp. 592-597.

[10] Herrmann, G. and I. C. Jong, "On Nonconservative Stability Problems of Elastic Systems with Slight Damping," J. Appl. Mech. 33, 1966, pp. 125-133.

[11] Nemat-Nasser, S. and G. Herrmann, "Some General Considerations Concerning the Destabilizing Effect in Nonconservative Systems," ZAMP 17, 1966, pp. 305-312.

[12] Nemat-Nasser, S., S. N. Prasad and G. Herrmann, "Destabilizing Effect of Velocity-Dependent Forces in Nonconservative Continuous Systems," AIAA J. 4, 1966, pp. 1276-1280.

[13] Nemat-Nasser, S., "On the Stability of the Equilibrium of Nonconservative Continuous Systems with Slight Damping," J. Appl. Mech. 34, 1967, pp. 344-348.

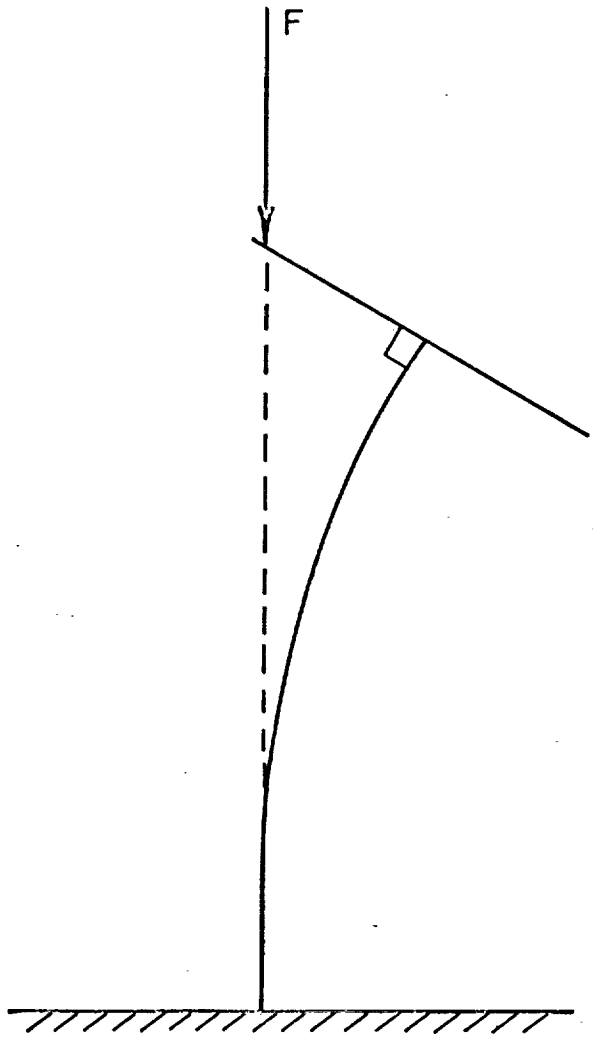

Fig. 1. Reut's problem

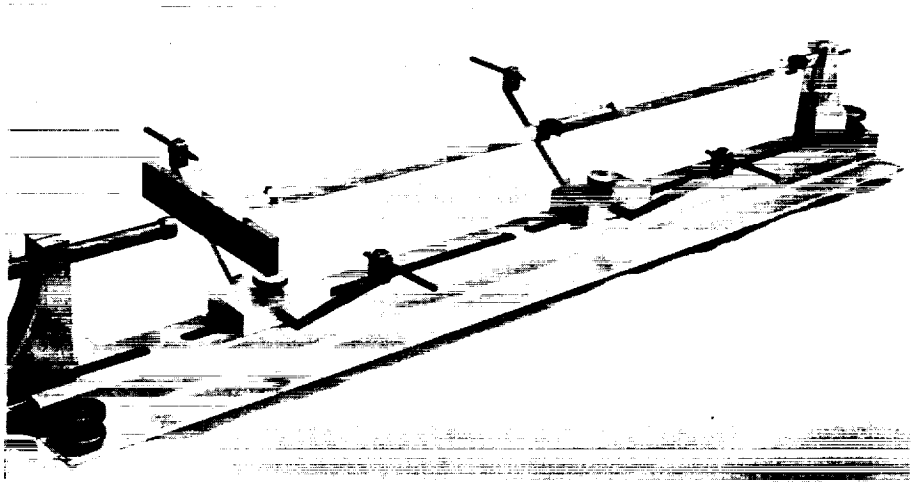

Fig. 2. Photograph of the model

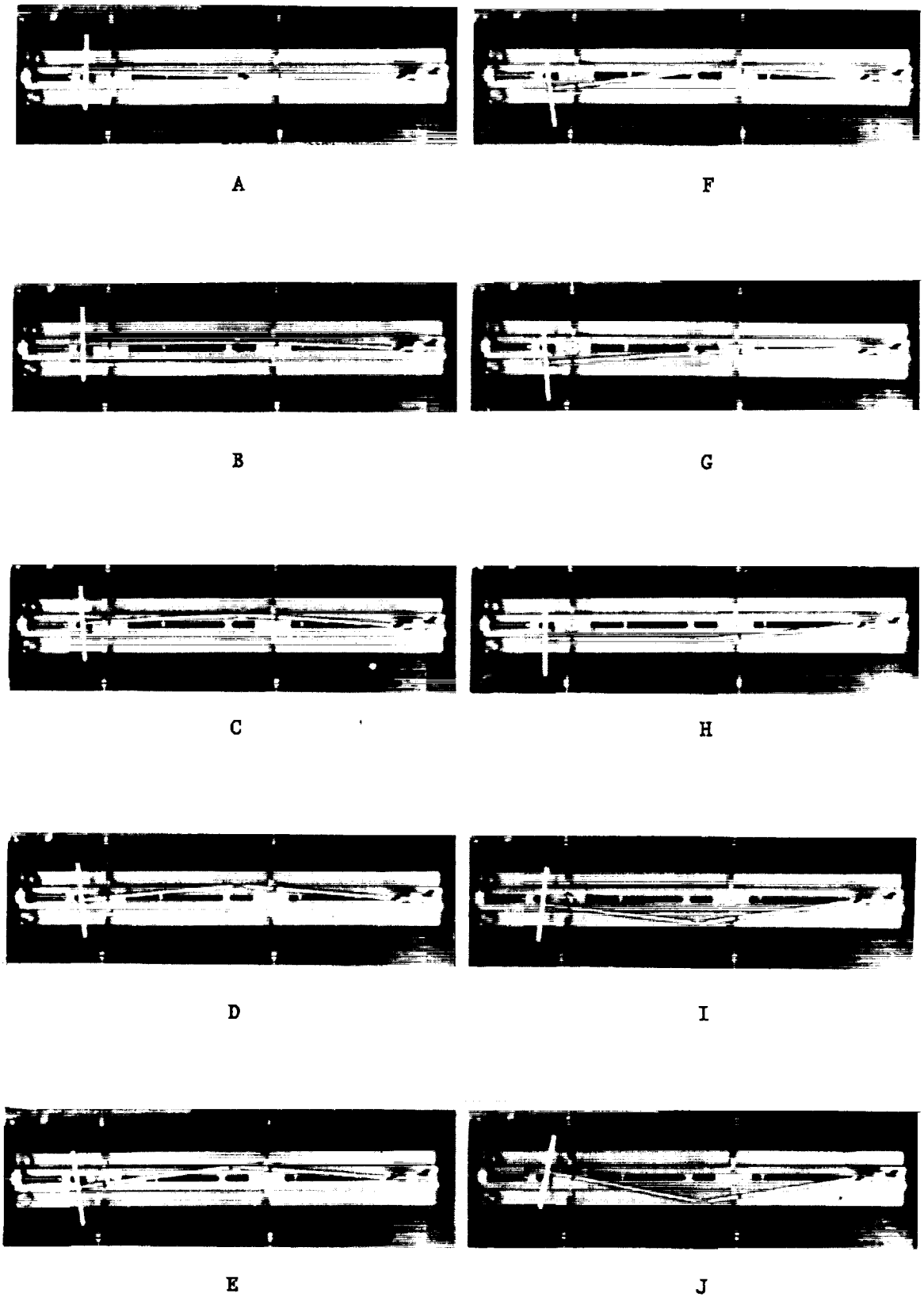

Fig. 3. Sequence of photographs depicting flutter

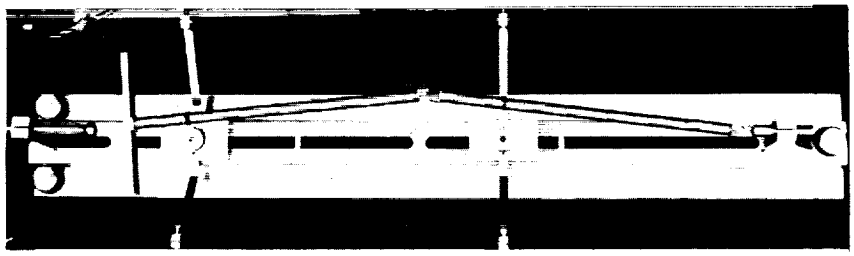

Fig. 4. Buckled state: divergence

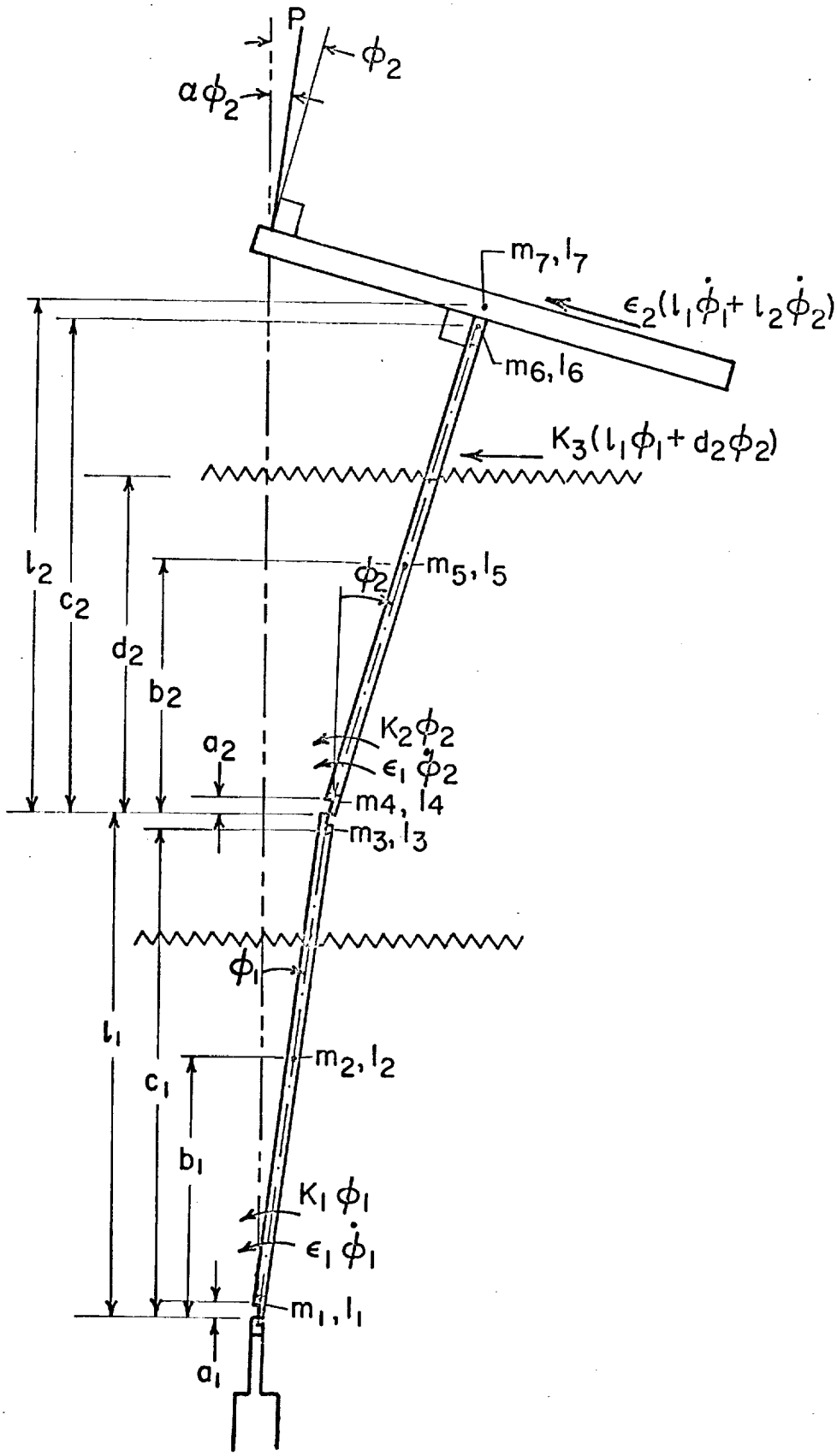

Fig. 5. Schematic of the model

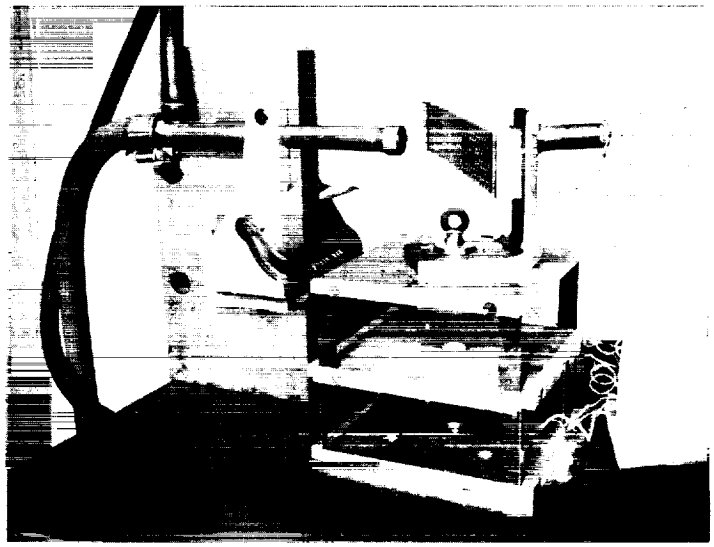

Fig. 6. Photograph of the calibrating system

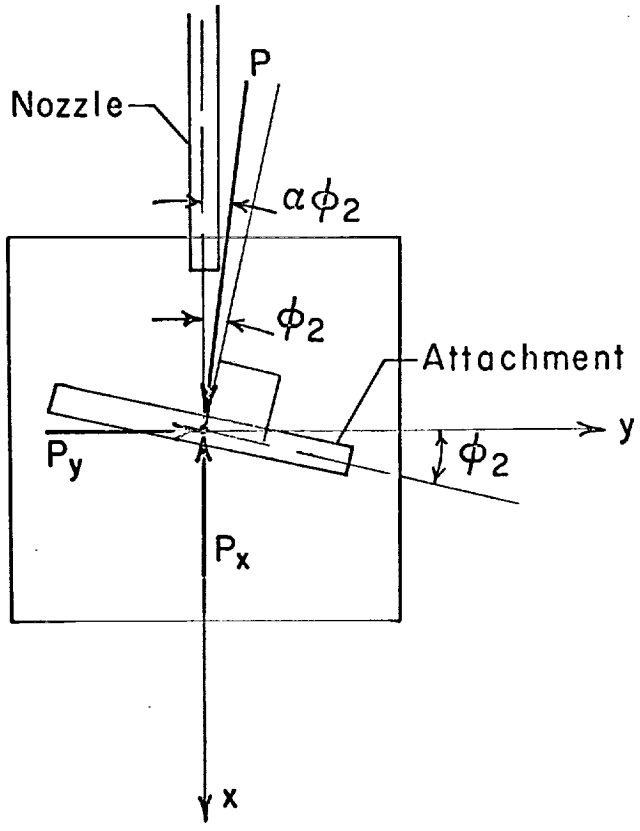

Fig. 7. Attachment mounted on calibrating system (top view)

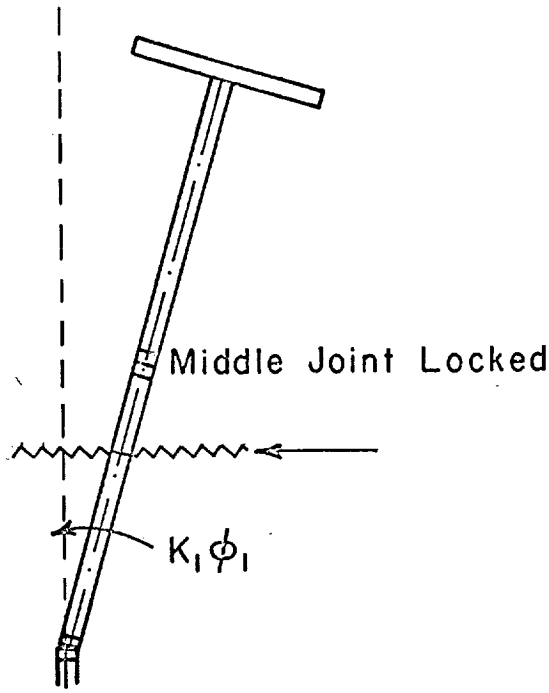

Fig. 8. Configuration to find K_1 by dynamic method

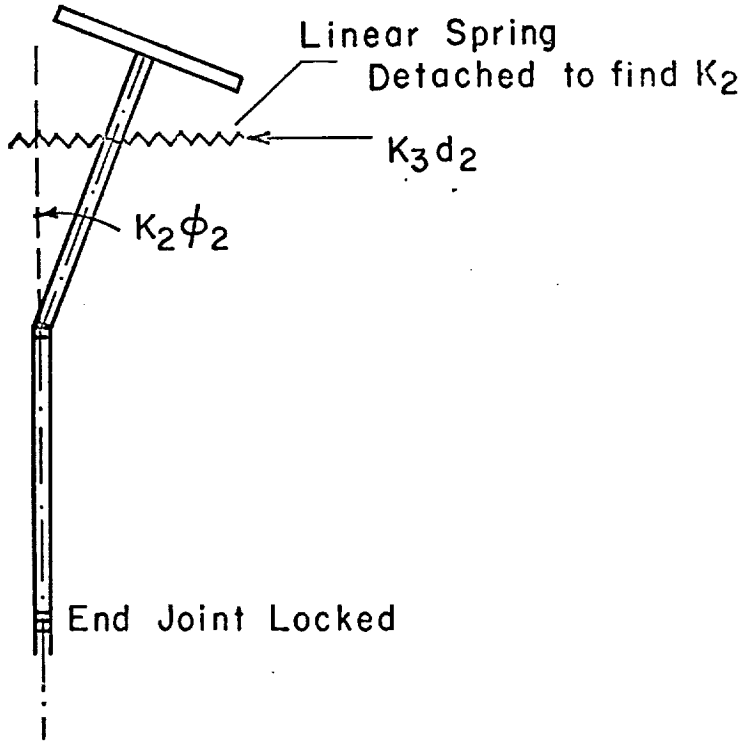

Fig. 9. Configuration to find K_2 and K_3 by dynamic method

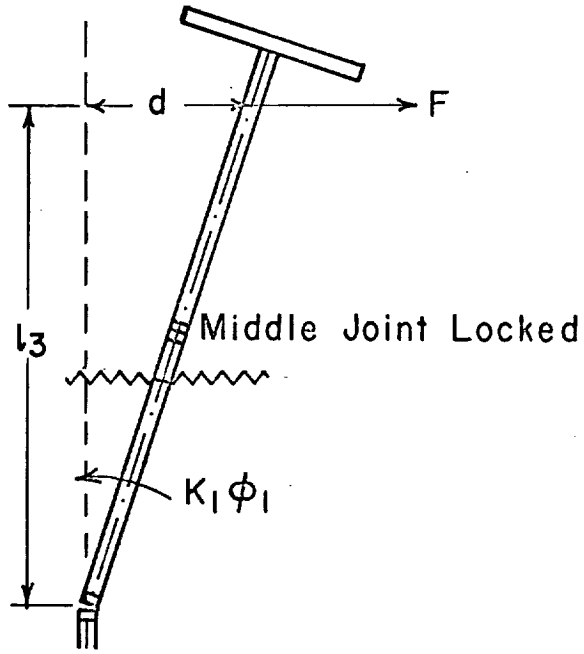

Fig. 10. Configuration to find K_1 by static method

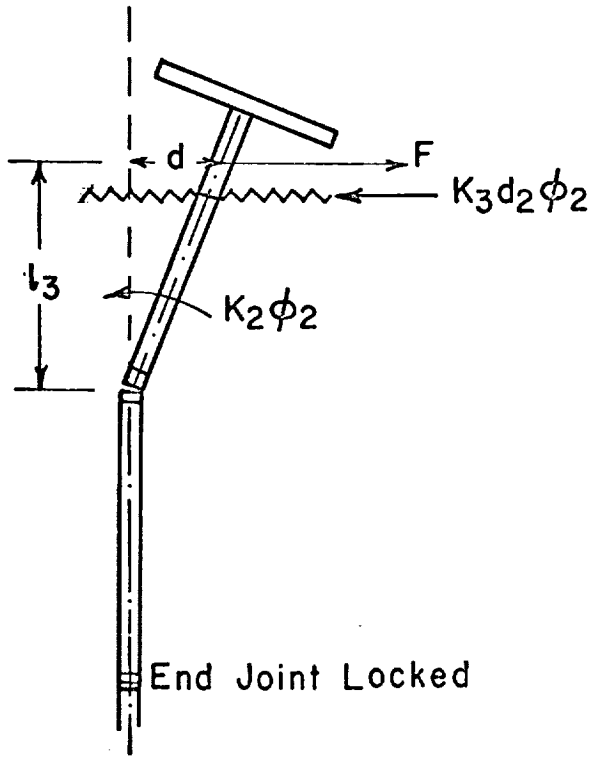

Fig. 11. Configuration to find K_2 and K_3 by static method

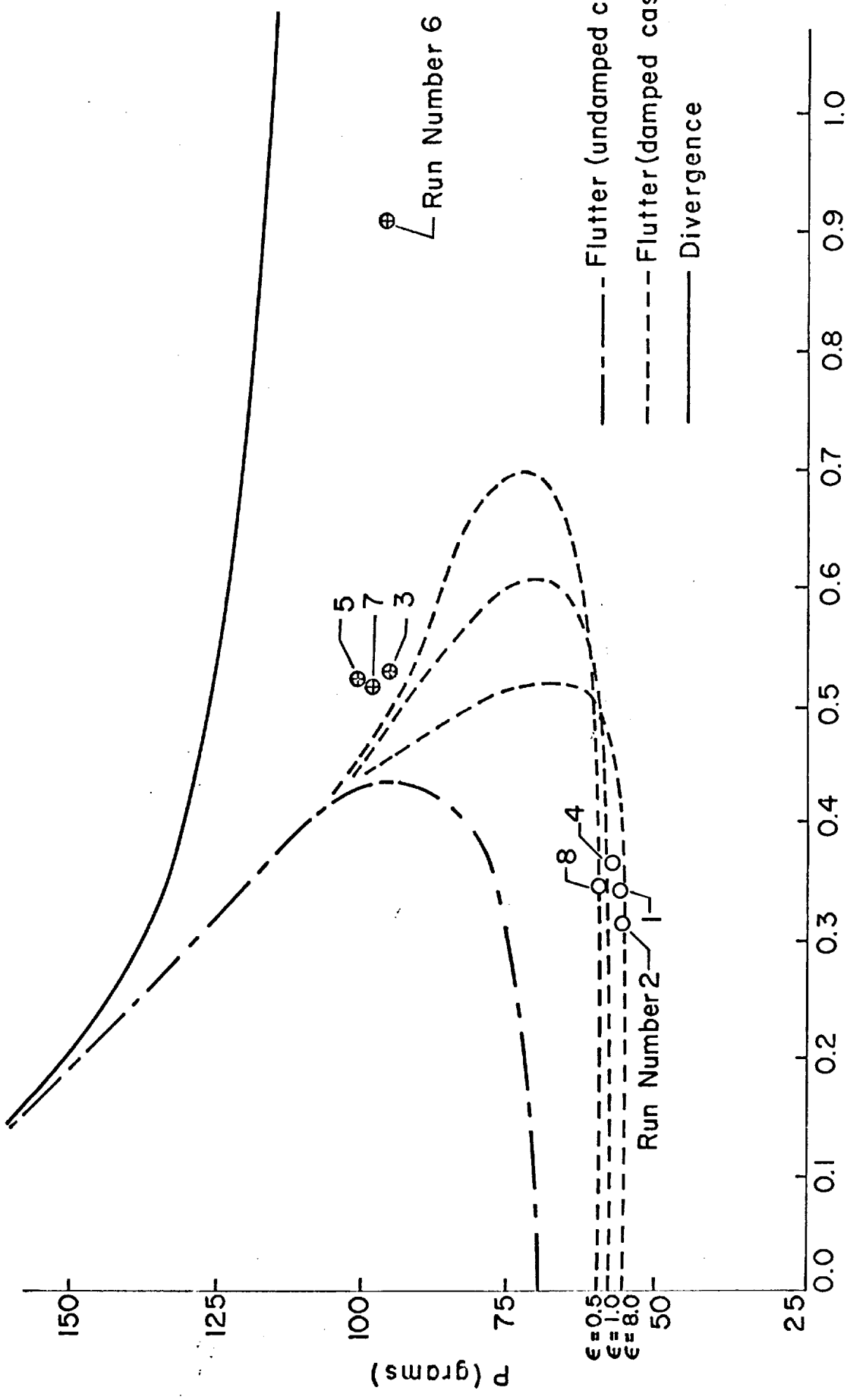

Fig. 12. Stability diagram - System I

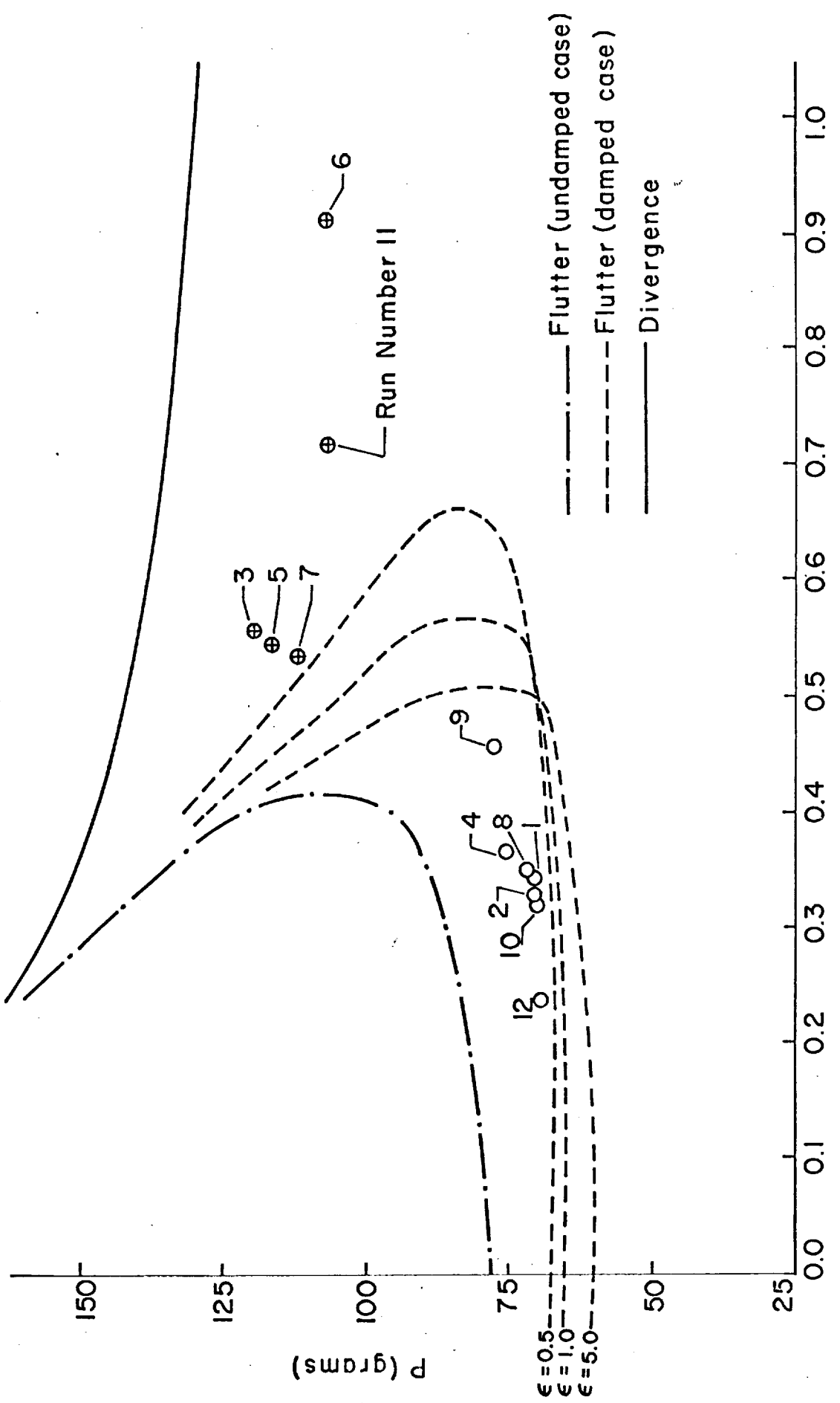

Fig. 13. Stability diagram - System II

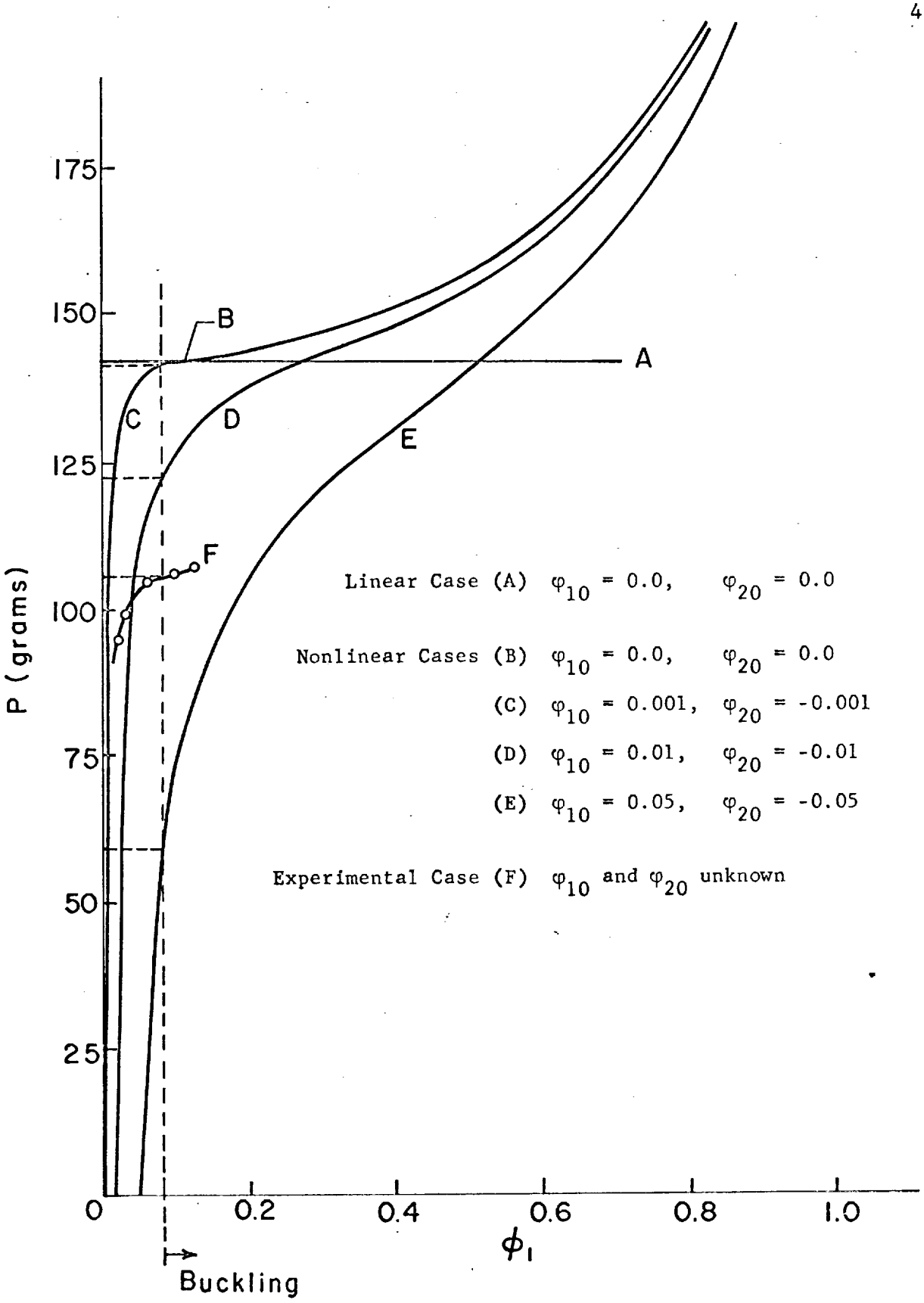

Fig. 14. Force versus deflection for nonlinear divergence theory with initial imperfections

TABLE 1

SYSTEM DATA

Dimensions (cm)	Part	Mass (gm)	Centroidal Moment of Inertia ($gm \cdot cm^2$)
$a_1 = 0.692$	1	10.20	~ 0
$b_1 = 16.3$	2	22.0	1655
$c_1 = 31.9$	3	42.1	~ 0
$a_2 = 0.692$	4	10.20	~ 0
$b_2 = 16.3$	5	22.0	1655
$c_2 = 32.3$	6	3.2	~ 0
$d_2 = 25.3$	7	43.5	771
$\ell_1 = 32.4$			
$\ell_2 = 32.6$			

Spring Constants		Dynamic Method	Static Method
System I	K_1	5.70×10^6 gm·cm	----
	K_2	9.12×10^6 gm·cm	----
	K_3	3.50×10^2 gm/cm	----
System II	K_1	5.34×10^6 gm·cm	5.45×10^6 gm·cm
	K_2	9.02×10^6 gm·cm	9.41×10^6 gm·cm
	K_3	3.35×10^2 gm/cm	3.53×10^2 gm/cm

TABLE 2

SUMMARY OF NUMERICAL RESULTS

		SYSTEM I						SYSTEM II					
		Experimental		Theoretical			% error	Experimental		Theoretical			% error
Run #	α	*	P_{crit} (gm)	1 (gm)	2 (gm)	3 (gm)		*	P_{crit} (gm)	1 (gm)	2 (gm)	3 (gm)	
1	0.343	F	56.4	72	55	---	+ 2.5	F	70.2	89	62	---	+12.9
2	0.327	F	55.2	70	55	---	+ 0.3	F	69.7	88	62	---	+11.1
3	0.560	B	94.9	--	--	124	-23.4	B	118.3	--	--	140	-15.1
4	0.368	F	57.2	73	55	---	+ 3.8	F	75.7	90	63	---	+19.2
5	0.548	B	99.9	--	--	125	-20.1	B	116.0	--	--	140	-17.0
6	0.913	B	95.9	--	--	117	-18.0	B	111.9	--	--	130	-13.8
7	0.533	B	97.9	--	--	125	-21.7	B	110.2	--	--	140	-21.3
8	0.346	F	58.8	77	55	---	+ 6.9	F	69.8	89	62	---	+11.4
9	0.454							F	77.0	--	66	---	+16.7
10	0.320							F	70.2	87	62	---	+12.9
11	0.717							B	105.0	--	--	135	-14.8
12	0.238							F	69.7	83	62	---	+12.4

* Observed loss of stability: F = flutter, B = buckling.

1 Undamped flutter.

2 Damped flutter, $\epsilon = 5.0$.

3 Buckling.